Available online at www.sciencedirect.com

ScienceDirect

Energy Procedia 35 (2013) 307 – 316

Energy Procedia

Deep Wind, 24–25 January 2013, Trondheim, NORWAY

Turbulence Measurements in Shallow Water from a Subsurface Moored Moving Platform

Mostafa Bakhoday Paskyabi[a,*], Ilker Fer[a]

[a]*Geophysical Institute, University of Bergen, Allégaten 70, N-5007 Bergen, Norway*

Abstract

Preliminary results are presented from a moored, autonomous instrument measuring the upper ocean turbulent dissipation rate together with the surface gravity wave field. Observations are made in the area approximately 30 km southwest of Bergen, Norway between 28 and 30 November 2012, at about 8 m from the surface in 20 m deep water. The platform is the top element of a bottom-anchored mooring line, and moves in response to currents and waves. Shear probes mounted on the nose of the platform allow measurements of dissipation rate of turbulent kinetic energy, ε, in the frequency range between 1 to 20 Hz in which shear probes are less contaminated by the surface gravity wave disturbances and platform motions. A high-resolution pressure sensor and an acoustic Doppler velocimeter allow estimates of surface bulk wave parameters and measurements of mean currents at a single depth. For the present deployment, in the shallow water within the wave-affected surface layer, at a depth of about 4 significant wave heights, good quality measurements of ε were limited by the instrument angle of attack and wave effects. Observations agree well with the scaling of dissipation due to wave breaking. Our preliminary results confirm that successful moored shear probes measurements are possible in the wave-affected layer of the upper ocean.

Selection and peer-review under responsibility of SINTEF Energi AS

Keywords: upper-ocean turbulence, autonomous platform, motion correction, dissipation rate of TKE, surface gravity waves, angle of attack, shear probe, wave breaking

1. Introduction

Turbulent processes and dynamics of the upper ocean play an important role in the momentum, heat, and energy exchanges across the air-sea interface. Measurements of the near-surface turbulent fluxes and kinetic energy are challenging, owing to the harsh environment for oceanographic sensors to efficiently operate, the contaminations and disturbances induced by platform motions and surface wave orbital velocities [1, 2]. Furthermore, surface gravity waves have considerable amount of energy that can substantially influence the design, operation, and maintenance of offshore wind power production facilities, fixed foundations, moving platforms, and oceanographic sensors. The presence of such disturbances, especially those induced by surface gravity waves, imposes complex requirements for the sensors and measurement technologies near

*Corresponding author
Email address: Mostafa.Bakhoday@gfi.uib.no (Mostafa Bakhoday Paskyabi)

1876-6102
Selection and peer-review under responsibility of SINTEF Energi AS
doi:10.1016/j.egypro.2013.07.183

the wavy sea surface, most commonly confining the measurements to the rate of Turbulent Kinetic Energy (TKE) dissipation, ε.

Conventionally, ocean microstructure is measured using air-foil shear probes and fast-response thermistors, see Lueck et al. (2002) [3] for a review. Typical near-surface turbulence studies include measurements of ϵ using shear probes mounted on a submarine [4] or free rising microstructure profilers [2]. Profiling measurements, however, cannot sample sufficiently in time, over the intermittent nature of turbulence, nor resolve the life cycle of wave breaking events. Time series measurements from a moored instrument are necessary. The first attempt of moored autonomous turbulence measurements by shear probes and thermistors was made by Lueck and Huang (1998) [5]. Their measurements, however, were made in a swift tidal channel, away from the surface layer. Although each approach (profiling and moored) offers different insights into the upper ocean turbulence variability, each has its limitations. For example, measurements from a fixed mooring platform typically rely on the conversion from frequency space into the wavenumber space, via Taylor's frozen hypothesis, that hinders an accurate estimation of ε due to existing overlap between the time scales of surface waves and the near surface turbulence [1].

In this study, we present observations of upper ocean microstructure made by the Moored Autonomous Turbulence System (MATS) [6, 7], from a short deployment southwest of Bergen, Norway, in late November 2012. The instrument is equipped with a set of oceanographic sensors that makes it possible to acquire long time series of pressure, mean current, small-scale 3D velocity fluctuations, small-scale shear and temperature gradient at a fixed level (in this application, about 8 m below the sea surface). Furthermore, an inertial motion package mounted on the platform allows for necessary corrections for the platform vibrations and motion-induced contaminations. Preliminary results from this deployment are presented here.

2. Observations, Conditions, and Methods

2.1. Data collection

Observations of ocean microstructure were made during the cruise of the Research Vessel Håkon Mosby between 28 and 30 November 2012. The measurement site is approximately 30 km southwest of Bergen in 20 m of water, less than 5 km close to the east of 200 m isobath of the Norwegian trench (Fig. 1). Ancillary atmospheric data were logged from the ship's meteorological mast at 15 m height.

MATS has been designed to collect long-time series of pressure, mean current, small scale turbulence velocity vector and temperature data at a fixed level. The details of the instruments, together with its com-

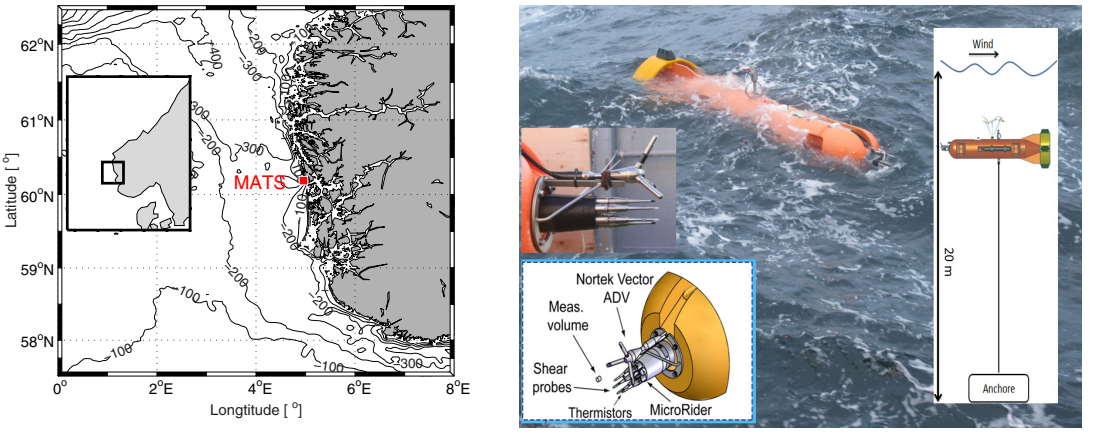

Fig. 1. *Left*) Map showing the study area and the location of MATS (red square). Isobaths are drawn at 100 m intervals. *Right*) Picture of MATS during deployment, together with a close up of the sensors (inset). The other insets (sketches) identify the sensors and the MATS mooring in the water column.

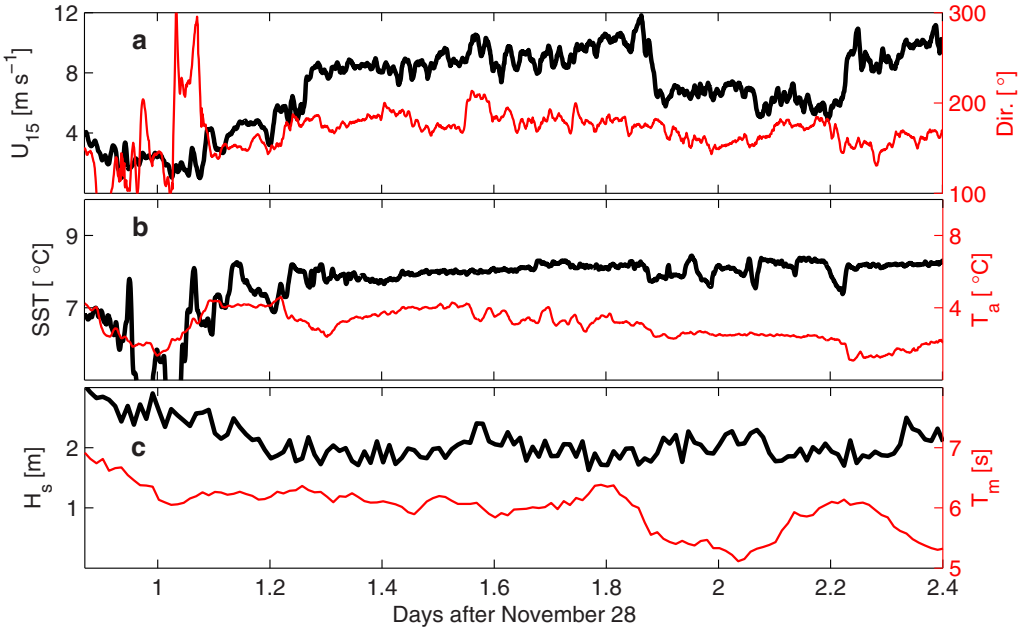

Fig. 2. Evolution of a) wind speed U_{15} together with the wind direction, positive clockwise from north, referred to the direction from which the wind is originating, b) sea surface temperature, SST, and air temperature at 15 m height, and c) the significant wave height, H_s, and mean wave period, T_m, measured by motion-corrected pressure data for the duration of the experiment.

ponents and processing techniques are given elsewhere [6]. Briefly, the platform is a low-drag buoy, StableMoor 400, custom modified by Flotation Technologies to fit the turbulence instruments. The buoy is equipped with a MicroRider turbulence instrument package consisting of two air-foil shear probes, two fast-response thermistors, a pressure transducer and a 3-axis accelerometer. An additional acoustic Doppler velocimeter (ADV), Nortek Vector, is interfaced with the MicroRider. The sensor head of the ADV is rigidly fixed to the buoy, as close as possible to the MicroRider sensors such that the temperature and 3D velocity are sampled at approximately the same measurement volume. Additionally a low-power 6D motion sensor, Gyrocube 3F (O-Navi), is fitted into the MicroRider. The entire system is powered by two rechargeable Lithium-Ion battery packs of 40Ah, each giving an estimated operating time of 450 h, requiring a memory capacity of 18 GB. The buoy is the upper element of a bottom-anchored mooring line, allowed to align with the current.

For this deployment, MATS was set to acquire data at approximately 8 m below the sea surface, sampling 15-min bursts followed by one minute of file book-keeping. In this study, we use the data measured by the shear probes to estimate ε.

2.2. Atmospheric forcing and surface waves

The wind speed (at 15 m height), U_{15}, and wind direction measured from ship's mast are shown in Fig. 2-a. The most frequently observed wind speed was about 9 m s^{-1}. Early in the deployment the conditions were calm, with about 2 m s^{-1}, and wind speed increased to 10 m s^{-1}, with approximately steady direction from southwest, creating unlimited fetch conditions. Typically the air temperature, T_a, was less than the Sea Surface Temperature (SST) suggesting conditions favorable for convection (Fig. 2-b).

Wave height and period are calculated using the pressure records from the high-resolution pressure sensor mounted on the MATS. Linear wave theory is used to convert the pressure spectra to the surface elevation spectra by including an extra correction for the platform motion [8]. The estimated spectra are

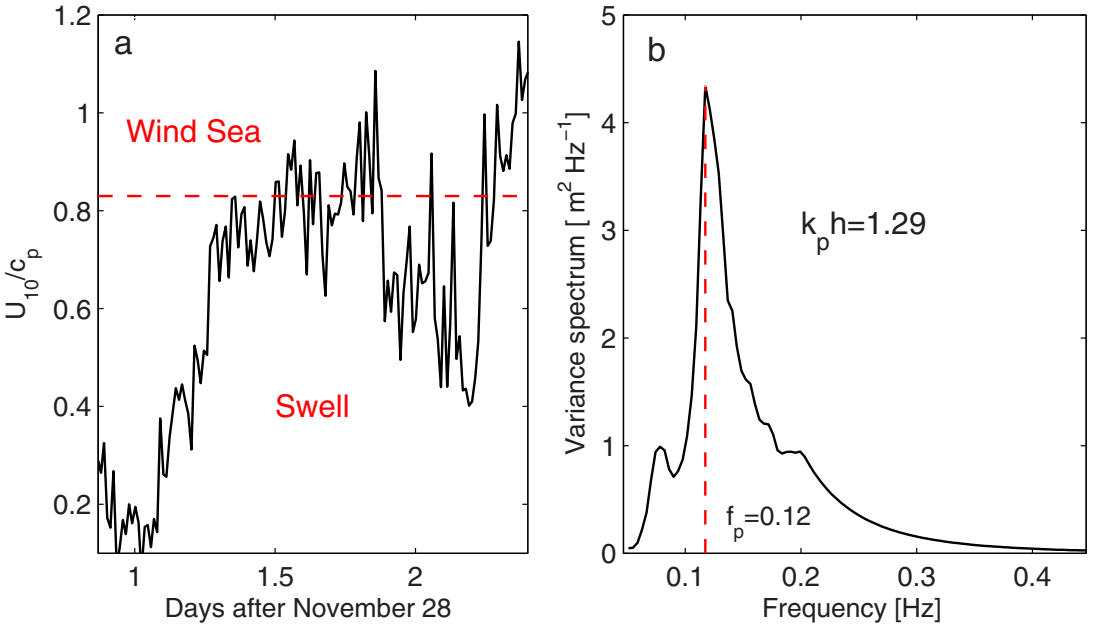

Fig. 3. a) Time series of the inverse of wave age (solid curve) and separation between swell and wind sea (dashed red line). b) Time-averaged wave energy spectrum estimated from the motion-corrected pressure data during the deployment. Dashed red line highlights the peak frequency, f_p.

extrapolated in the equilibrium range, with an f^{-5} slope beyond an identified cut-off frequency where higher frequency measurements are not reliable. Waves with mean periods, T_m, of approximately 6 s and significant wave height, H_s, between 2 and 3 m were apparent during the experiment (Fig. 2-c). The wave conditions, based on the linear wave theory, can be characterized with a mean non-dimensional depth of $k_p h = 1.29$ (where k_p is the peak wavenumber (Fig. 3-b)) and wave age (peak wave phase speed normalized by the wind speed at 10 m height, c_p/U_{10}) ranging from 0.9 to 16, i.e. a combination of both young and old seas (Fig. 3-a). Measurements of wind at 15 m height are corrected to U_{10} using the COARE 3.0 algorithms [9]. Donelan et al. (1993) [10] proposed that for the inverse wave age of $U_{10}/c_p = 0.83$, the wave spectrum is at full development, whereas below and above this value, sea is identified as swell and wind sea, respectively. During our experiment, 76% of the time the inverse of wave age was below 0.83.

2.3. Methods

Reliable measurements using shear probes require a small angle of attack (AOA). When instantaneous current past the sensor is not along the axis of the probe, but has an AOA, $\alpha > 20^\circ$, the potential theory used by the shear probes to measure hydrodynamic lift forces breaks down, and the measured shear may deviate substantially from the true one.

For the MATS's shear probes, a first estimate of AOA can be given as

$$\alpha = \alpha_{lf} + \alpha_{hf} = \arctan\left(f_{corr}(\alpha, \Theta, \theta, A_x, A_y, A_z) \frac{W}{u_h} \right), \tag{1}$$

here $f_{corr} \approx 1$ is the AOA correction factor, Θ is the mean current direction, and u_h is the segment-averaged current along the axis of the platform. Three components of the platform accelerations measured by accelerometer sensors are denoted by A_x, A_y, and A_z, respectively, and and α_{lf} and α_{hf} are the low-frequency and high-frequency estimates of α. U, V and W are the horizontal and vertical components of the mean

current, respectively. Fer and Bakhoday–Paskyabi (2013) [6] showed that the high-frequency estimate of AOA can be successfully used to identify good quality data, using α_{hf} within ±7° (Fig. 9-b). In addition to the AOA, when estimating ε using shear probes, the applicability of the Taylor's hypothesis must be confirmed. Especially at times when the mean current is weak, the wake induced by oscillating motions of surface gravity waves or the secondary currents induced by the platform body cannot be advected past the sensors, violating the Taylor's frozen turbulence hypothesis. Using 60-s long segments of MATS data, Fer and Bakhoday–Paskyabi (2013) [6], suggest that when the ratio

$$R = \left| \frac{u}{u_{wave}} \right| \tag{2}$$

is sufficiently greater than unity, dissipation rates can be measured with reasonable accuracy. Here u_{wave} is the wave induced flow calculated by integrating the velocity spectra in the wave dominated regions (frequency band corresponding to periods between 1 s to 20 s), and u is the mean flow measured by the ADV. In their deployment, for $R > 1.3$ the measurement volume was flushed sufficiently with no apparent bias for dissipation measurements. For the present deployment, a scatter diagram of dissipation rates against R (not shown) suggests that $R > 1.1$ is sufficient to delineate segments suspect to Taylor's hypothesis. In summary, we split each 15-min burst into 60-s long segments and retain the segments for analysis when $|\alpha_{hf}| < 7°$ and $R > 1.1$.

After removing the parts of shear signals coherent with the accelerometer data using the method devised by Goodman et al. 2006 [11] (Fig. 7), the dissipation rate of TKE for the 60-s long segments satisfying the aforementioned Quality Control (QC) criteria at each burst is measured using the equation for the isotropic turbulence:

$$\varepsilon_i = \frac{15}{2}\nu\overline{\left(\frac{\partial u_i}{\partial x}\right)^2} = \frac{15}{2}\nu\int_{k_0}^{k_c}\psi_i(k)dk, \tag{3}$$

where ψ_i is the shear spectrum measured by the ith ($i = 1, 2$) probe, k denotes wavenumber, ν is the viscosity as a function of the local water temperature, and u_i identifies the ith shear probe data ($u_1 = w$ and $u_2 = v$). The integration of the shear spectra between a lower integration limit, k_0, and the Kolmogorov wavenumber, $k_c = (\varepsilon/\nu^3)^{1/4}$, yields the corresponding shear variance. The wavenumber is calculated using Taylor's hypothesis and the mean current speed of the flow obtained from ADV at each 60-s long segment. In practice, due to the constraints in the the wave-affected upper layer, k_0 is typically 4-5 cpm and the upper limit is obtained by an iterative algorithm to calculate ε by integrating the shear spectra [6]. The unresolved wavenumbers of spectrum are accounted for using the variance from the Nasmyth universal spectrum:

$$\psi_{nas}(k) = 8.05\frac{(k/k_c)}{1 + (20 \times k/k_c)^{3.7}}. \tag{4}$$

The level of dissipation rate and its evolution in time are not trivial to interpret. For comparison with the measured ε by shear probes, we also present, for reference, dissipation rates predicted from low-of-the-wall (LOW) and from a scaling for the wave-affected surface layer suggested by Terray et al. (1996, T96) [12]. The LOW model for the dissipation rate in the surface layer of a flat, wall boundary layer is given by

$$\varepsilon = \frac{u_{*w}^3}{\kappa|z|}, \tag{5}$$

where u_{*w} is the water-side friction velocity, κ is von Kármán's constant, and z denotes the distance from wall (here, depth measured from the sea surface). T96 assumed that the vertical integrated ε in the water column is approximately equal to the mean energy input flux from the wind to the ocean. They suggested scaling of ε using the estimated wind energy input, F, significant wave height, H_s, and the depth below the sea surface, z:

$$\varepsilon = 0.3\frac{FH_s}{z^2}, \tag{6}$$

where $F = \beta u_{*w}^3$ and β is a wave-age-dependent parameter (here $\beta = 250$ following [6]).

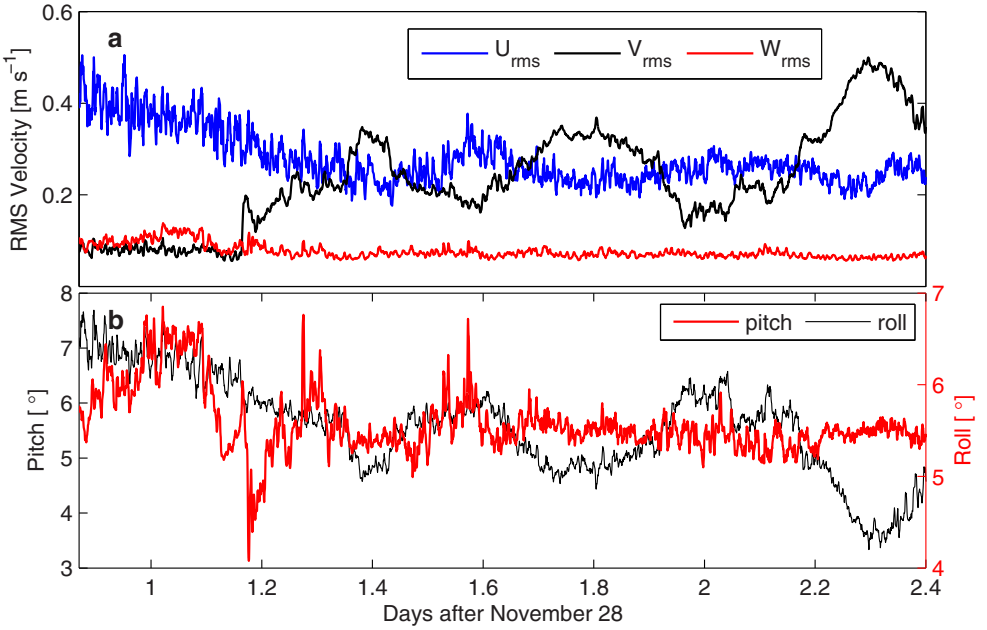

Fig. 4. Time series of: a) the rms current velocities, U_{rms}, V_{rms}, and W_{rms}, respectively, determined from ADV with sampling frequency of 8 Hz for the period of deployment, and b) pitch, θ and roll, ϕ, measured by the motion sensor.

3. Preliminary Results

Figure 4-a shows the root-mean-square of velocity components calculated at each 60-s segment ($U_{rms}(t)$, $V_{rms}(t)$, and $W_{rms}(t)$) recorded by the ADV on the MATS during the period of deployment. Here $Oxyz$ is body coordinate frame, with Ox pointing along the axis, Oy pointing toward port, and Oz vertically upward when the MATS is horizontal. Early in the deployment, the first six hours, the mean flow is weak and the wave rms velocities dominate the flow. During this period U_{rms} is 3-4 times larger than U, and flow reversals occur. For the rest of the deployment, the along axis flow closely follows U_{rms} within a factor of 1.2 (hence not shown). Large transverse velocity variations, apparent in V_{rms}, lead to significant stretches of data which do not satisfy the Taylor's hypothesis when the along axis flow was relatively weak. The variability of V_{rms} is coherent with the platform pitching (Figs. 4-b). The U_{rms} (and also U) oscillated at 4-6 hour period suggesting significant third or fourth harmonic semi-diurnal tidal variability. The vertical component W_{rms} remained nearly constant throughout the deployment. Pitch, θ, and roll, ϕ, measured by the motion sensor are shown in Fig. 4-b. Although, roll is relatively constant in time with an average value of $\phi = 5.8°$, pitch shows strong oscillations in response to the currents, and wind and wave forcing.

Velocity spectra inferred from ADV ($P_{uu}(f)$, $P_{vv}(f)$, and $P_{ww}(f)$, where f is the frequency in Hz) are shown for a selected 15-min burst where the spectral calculation is made over an fft length of 256 s. At frequencies more than 0.5 Hz, the ADV shows an approximately constant noise floor that is lower for the axial component due to the configuration of the acoustic beams (Fig. 5-a and b). Velocity spectra in Fig. 5-a and b indicate also energetic wave motions at frequencies between approximately 0.05 and 1 Hz. Due to low frequency contamination by waves and high frequency noise levels, the inertial subrange cannot be detected. Thus, it is ill-advised to use ADV data to measure ϵ using the eddy-correlation technique and the inertial subrange method.

The time series from the shear probes, $\partial w/\partial x$ and $\partial v/\partial x$, are shown in Figs. 6-a and b, respectively, for the same used for the spectra in Fig. 5 (but a 2-min long segment). The corresponding time series for the signals recorded by the mounted accelerometers are shown in Figs. 6-c and d. The shear and

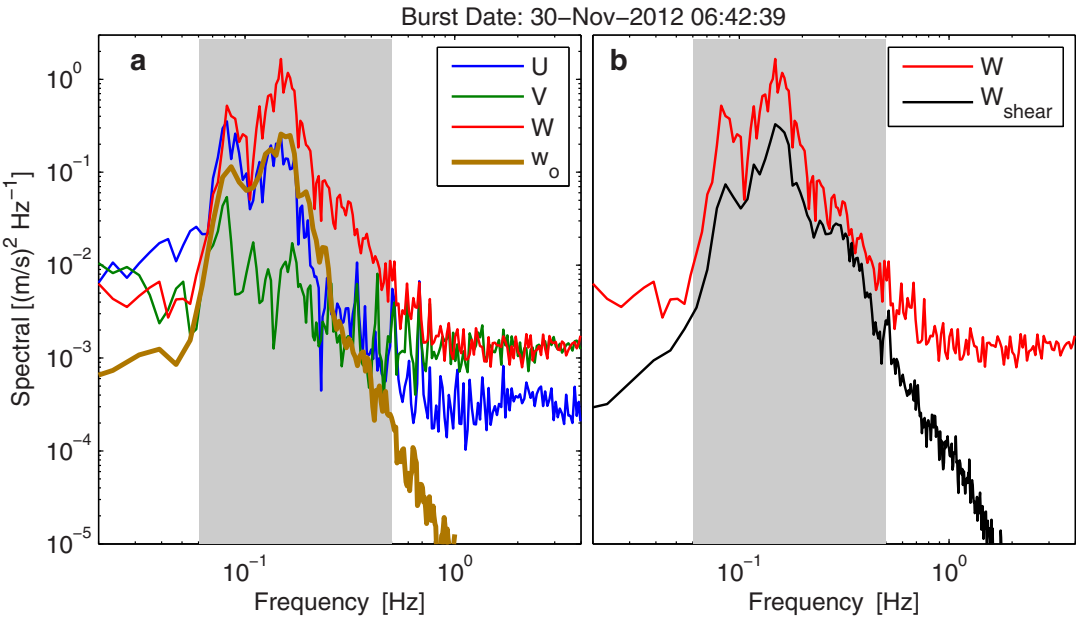

Fig. 5. a) Frequency spectrum of U, V, and W velocities measured by the ADV for a 15-min burst starting from 30 Nov 2012, 06:42:39 UTC. The spectra are band-averaged in frequency in $\log_{10}(\Delta f) = 0.01$ bins. Also shown is the vertical component of wave orbital velocity spectrum, W_o, and b) comparison between the integrated spectra of the shear probe 1 data, W_{shear}, and the vertical velocity component, W measured by the ADV for the same burst (dashed line and solid line, respectively)

accelerometer data from the two-axis vibration sensors were recorded at a sampling frequency of 512 Hz. The anomalies are apparent in the shear time series that primarily can be explained as a result of using Taylor's hypothesis and energetic wave motions. The large anomalies in the accelerometer signals are induced by the wave motion at the depth of MATS. It should be noted that the coherent behavior between shear probe signals and the accelerometer data are removed (Fig. 7 sh1-clean) using Goodman et al. 2006 [11] method. Furthermore, we use only the shear probe 1 data ($\partial w/\partial x$) to measure ε in this study.

The integrated signal from the shear probe can be compared to the the axial component of ADV velocity. Figure 5 shows the comparison between spectra of integrated shear probe, W_{shear}, and the vertical velocity component, W for a 15-min burst. This comparison represents the high correlation of the two spectra, especially at frequencies between 0.05 and 1 Hz energized by the wave motions. There is a time-lag between W_{shear} and W (calculated using cross correlation in time space) that can be described as the time for an eddy to be advected toward the shear probes from the ADV sampling volume (not shown here).

The shear wavenumber spectra of probe 1 for 60-s long segment from the same 15-min burst are shown in Fig. 7, together with the spectra from the vibration sensors (VA_x and VA_y) and the Nasmyth universal spectrum. The frequency domain shear spectra are converted into the wavenumber domain using the Taylor's hypothesis and using the average velocity over the 60 s window. Between the low-wavenumber wave-induced motions and the high-wavenumber vibrations and noise apparent in the spectra, there is a wavenumber band (in this example between 8 to 80 cpm) where both cleaned (sh1-clean) and raw (sh1) spectra conform with the Nasmyth's universal form. This agreement with the Nasmyth's form can be more clearly seen in the ensemble-averaged shear spectra (Fig. 7-b).

Figure 8 shows the different QC criteria applied in this study to accept dissipation rate measurements. The ratio between the mean flow to the wave-induced flow is shown in Fig. 8-a together with the region (gray) with good quality data. Due to the use of the high frequency portion of shear data to measure ε, the high frequency component of AOA is relevant for the flow past the sensor in deriving shear measurements from the raw data (Fig. 8-b). This figure also shows an inverse correlation between R and α_{hf}.

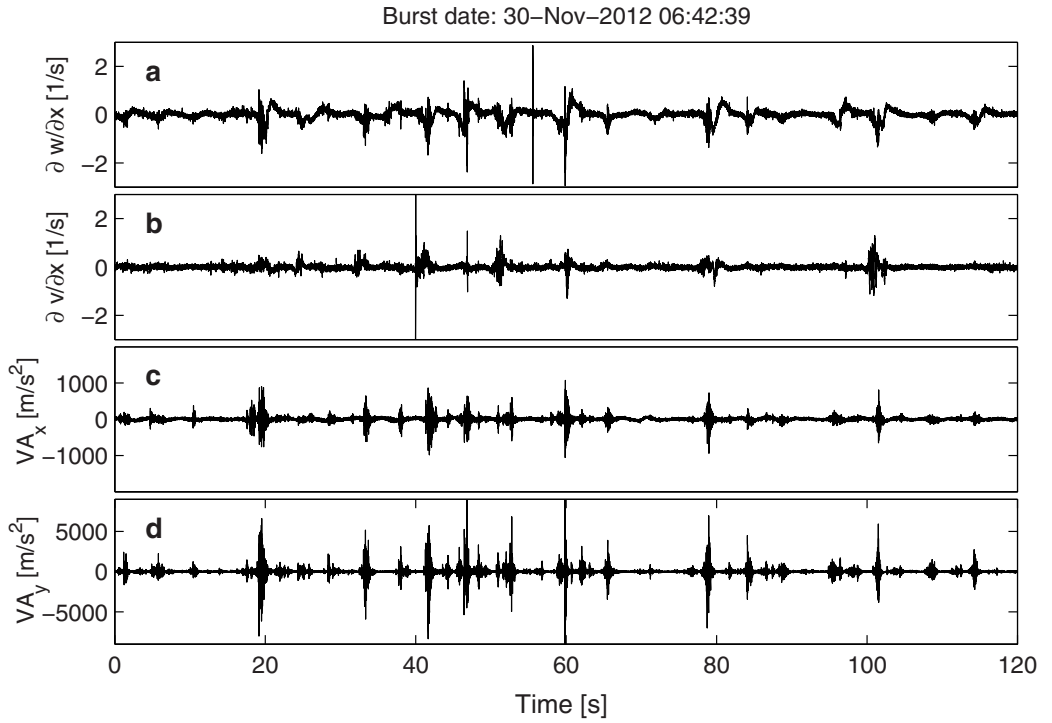

Fig. 6. Time series of the shear probes and accelerometer data from two-axis vibration sensors, VA_x and VA_y, respectively, for a 2-min burst starting from 30 Nov 2012, 06:42:39 UTC: a) shear probe 1, b) shear probe 2, c) VA_x, and d) VA_y.

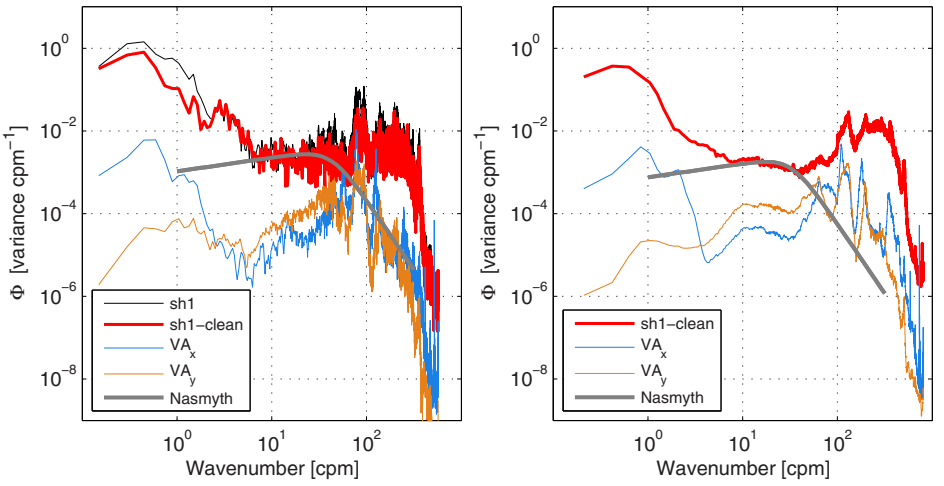

Fig. 7. a) Spectra from one 60-s long segment starting from 30 Nov 2012, 06:45 UTC. For this segment, $\varepsilon = 10^{-6}$ W kg^{-1}, $u = 0.45$ m s^{-1}, $R = 2$, $\alpha_{hf} = 3°$. Shown are the raw (sh1) and clean (sh1-clean) shear spectra and acceleration spectra from vibration sensors, VA_x, VA_y, respectively, together with the Nasmyth universal spectrum (gray). b) Spectra averaged over 51 ensembles selected when ε is between 1 and 2×10^{-6} W kg^{-1}. Averaged over the 51 ensembles, $u = 0.32$ m s^{-1}, $R = 1.75$, $\alpha_{hf} = 4.6°$ and $\varepsilon = 1.3\times10^{-6}$ W kg^{-1}.

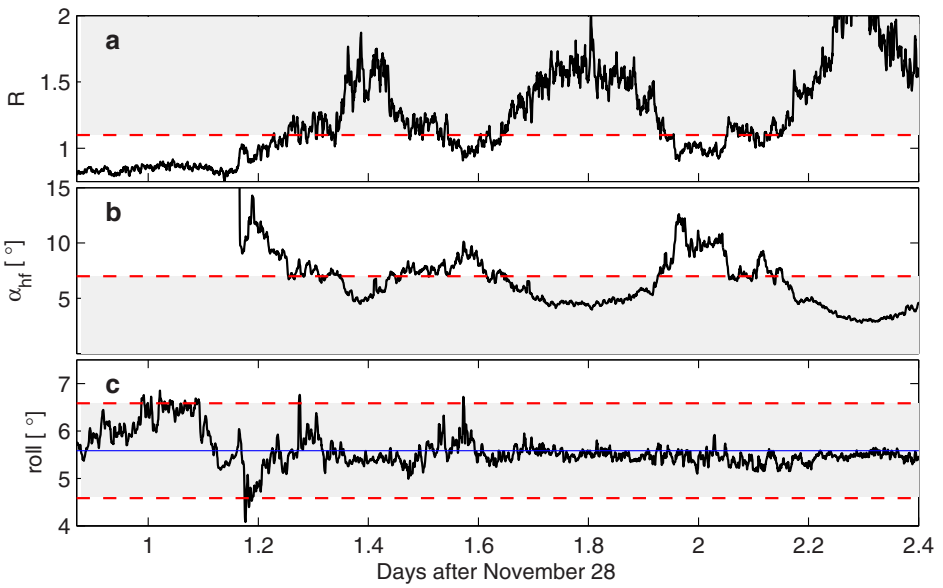

Fig. 8. Time series of a) the ratio of the mean flow to the wave-induced flow, R, using Eq. (2), b) the inferred high frequency component of angle of attack, α_{hf} that is calculated by integrating the α in the frequency band 0.5 to 2 Hz at each 60 s long segment, and c) platform's roll angle. Gray regions (dashed lines) indicate the thresholds for good quality measurements during the course of the experiment.

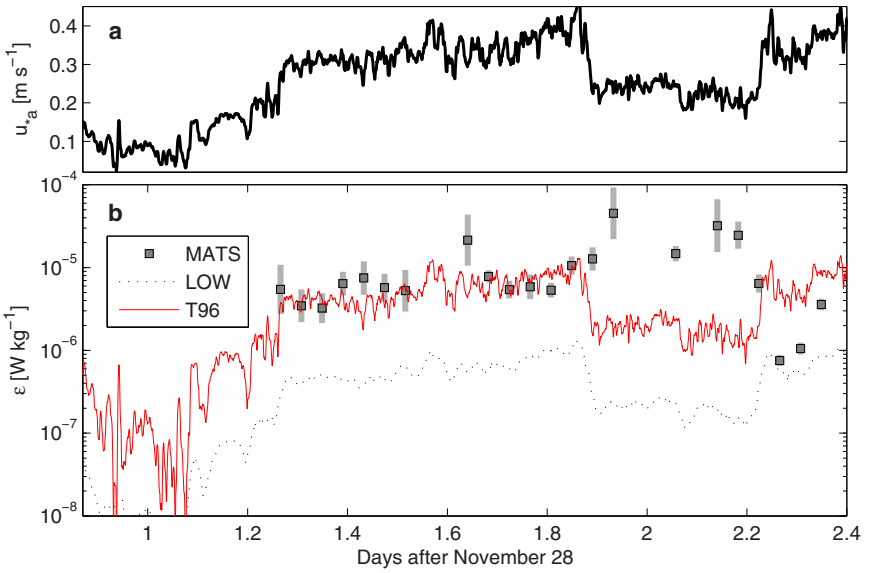

Fig. 9. Time series of a) air-side friction velocity, u_{*a}, and b) hourly averaged dissipation rate of TKE (markers) together with the %95 confidence intervals (gray bars). Also shown are the dissipation values predicted by the T96 scaling (red) and the LOW (dashed).

To measure ε, we apply Eqs. (3) and (4) to all 60-s long segments at each burst satisfying the QC criteria and mean roll less than 1°. The hourly average measured ε together with the %95 confidence limits are shown in Fig. 9-b. Also shown are the LOW and T96 predictions of dissipation rate as important diagnosis and reference tools for near the sea surface measurements of ε. The results show that ε measured at $z \sim (4-5)H_s$ is enhanced in the presence of surface gravity waves over those expected beneath the rigid boundaries.

4. Summary

A moored autonomous platform has been developed to obtain time series measurements of pressure, currents, small scale velocity and temperature fluctuations and small scale shear at a target depth below the sea surface. The platform is not a rigid, fixed frame, but moves in the water column, around its target depth, in response to currents and wave induced motions. For a mission off southwest of Bergen during 28–30 November 2012, data from a shear probe, the accelerometers, pressure sensor, and the Doppler velocimeter were utilized to measure surface wave bulk parameters, background mean current velocity components, and the dissipation rate ε of turbulent kinetic energy. Before measuring dissipation rate using the shear probe, substantial quality control should be employed mainly due to instability of platform, wave orbital velocity disturbances, and flow distortion. The resulting dissipation rate was consistent with the predictions of ε by the scaling of Terray et al. (1996) [12] that relates ε to wind energy input, significant wave height, and distance to the sea surface. The Doppler velocimeter mounted on the platform could not be used to measure ε due to both low and high frequency noise levels induced by mechanical vibration, platform motion, and flow distortion. Shear probes on a moored instrument provide for a promising means of measuring time series of dissipation rate in the upper ocean, however, further investigations in terms of wave and turbulence separation, flow distortion, and contaminations induced by platform motions are merited.

5. Acknowledgements

This work has been funded by the Norwegian Centre for Offshore Wind Energy (NORCOWE) under grant 193861/S60 from the Research Council of Norway (RCN).

References

[1] A. Soloviev, R. Lukas, Observation of wave-enhanced turbulence in the near-surface layer of the ocean during toga coare, Deep-Sea Research 50 (2003) 371–395.
[2] A. Anis, J. N. Moum, Surface wave-turbulence interactions. scaling $\epsilon(z)$ near the sea surface, J. Phys. Oceanogr. 25 (1995) 2025–2045.
[3] R. G. Lueck, F. Wolk, H. Yamazaki, Oceanic velocity microstructure measurements in the 20th century, J. of Oceanog. 58 (2002) 153–174.
[4] T. R. Osborn, D. M. Farmer, S. Vagle, S. A. Thorpe, M. Cure, Measurements of bubble plumes and turbulence from a submarine, Atmos. Ocean 30 (1992) 419–440.
[5] R. Lueck, D. Huang, Dissipation measurement with a moored instrument in a swift tidal channel, J. Atmos. and Ocean. Tech. 16 (1998) 1499–1505.
[6] I. Fer, M. Bakhoday-Paskyabi, Autonomous ocean turbulence measurements with a moored instrument, submitted in J. Atmos. Ocean. Technol.
[7] M. Bakhoday-Paskyabi, I. Fer, Turbulence structure in the upper ocean: a comparative study of observations and modelling, under revision in Ocean. Dyn.
[8] M. Bakhoday-Paskyabi, I. Fer, K. Christensen, Subsurface measurement of ocean surface gravity waves with a moving moored platform.
[9] C. W. Fairall, E. F. Bradley, J. E. Hare, A. A. Grachev, J. B. Edson, Bulk parameterization of air–sea fluxes: Updates and verification for the COARE algorithm, J. Clim. 16 (2003) 571–591.
[10] M. A. Donelan, F. W. Dobsond, S. D. Smith, On the dependence of sea surface roughness on wave development, J. Phys. Oceanogr. 23 (1993) 2143–2145.
[11] L. Goodman, E. R. Levine, R. G. Lueck, On measuring the terms of the turbulent kinetic energy budget from an auv, J. Atmos. and Ocean. Tech. 23 (2006) 977–990.
[12] E. A. Terray, M. A. Donelan, Y. C. Agrawal, W. M. Drennan, K. K. Kahma, A. J. Williams, P. A. Hwang, S. A. Kitaigorodski, Estimates of kinetic energy dissipation under breaking waves, J. Phys. Oceanogr. 26 (1996) 792–807.